Journal of Materials Chemistry A

Accepted Manuscript

ROYAL SOCIETY OF CHEMISTRY

www.rsc.org/materialsA

Journal of Materials Chemistry A

ARTICLE

Stable Inverse Opal Structure of Cadmium Chalcogenide for Efficient Water Splitting

Received 00th January 20xx,
Accepted 00th January 20xx

DOI: 10.1039/x0xx00000x

www.rsc.org/

Yi-Ren Lu,[‡] Peng-Fei Yin,[‡] Jing Mao, Meng-Jiao Ning, Yu-Zhu Zhou, Cun-Ku Dong, Tao Ling,[*] and Xi-Wen Du[*]

Cadmium chalcogenide nanocrystals (CCNCs) are regarded as promising materials for photoelectrochemical (PEC) water splitting. However, the relatively low PEC response and poor stability restricts their practical application. In the present work, we demonstrate that a well-designed inverse opal structure (IOS) composed of CCNCs can achieve an unprecedently high photocurrent and hydrogen production rate. Particularly, the IOS electrode keeps stable during 3 h continuously illumination, which is even superior to those photoanodes with surface passivation and/or co-catalysts. Quantitative investigation illuminates that IOS possesses high charge-separation efficiency and light-absorption capacity, which eventually results in the excellent PEC performance.

Introduction

Photoelectrochemical (PEC) splitting of water into hydrogen by the direct use of sunlight is an attractive and sustainable solution to the energy crisis and environmental problems.[1-6] Since the pioneering work of Honda and Fujishima,[6] tremendous efforts have been made to enhance the solar-to-hydrogen conversion efficiency (STH) of PEC cells. The exploitations of new light harvesters[3,4,7] and electrode configurations[8-10] are considered as two crucial aspects for enhancing overall efficiencies and device stabilities.

Recently, cadmium chalcogenide nanocrystals (CCNCs), have attracted extensive attention owing to their adjustable band gap,[11,12] high extinction coefficient,[13] and possible multiple exciton generation.[14] Therefore, they are highly expected to be light harvesters in PEC cells.[15-18] Nevertheless, the obtained STH efficiency of such materials are much lower than the theoretical value due to the drastic electron-hole recombination caused by the slow minor carrier (hole) transfer kinetics at the semiconductor/liquid interface.[17,18] More importantly, the accumulated holes can cause serious anodic corrosion, which deteriorates the stability of the photoelectrodes.[16,17]

The common strategies to overcome these problems include constructing heterojunction,[17-19] adopting surface passivation,[18] and adding co-catalysts[17] so as to enhance the hole transfer and reduce the charge recombination. Recently, Seol *et al.* employed IrO_x catalyst to modify the CCNCs-sensitized ZnO nanowires, and achieved an enhanced photocurrent which kept stable after 3 h illumination.[17] Even so, the PEC response and stability of CCNCs are still not satisfactory, which seriously limits their practical applications in PEC devices.

Another possible solution is to construct three-dimensional (3D) architectures, e.g. inverse opal structure (IOS), with CCNCs. As shown in Scheme 1, IOS possesses several unique advantages. First, the periodically 3D ordered structure provides well control of the incoming light via back reflections,[17] multi-scattering,[20] and surface resonance,[21,22] causing intensive light absorption. Second, the thin walls of IOS can dramatically reduce the diffusion length of holes, thus facilitating the charge separation and depressing the carrier recombination.[23] Third, the continuous walls offer direct pathways for photo-generated electrons in CCNCs. Fourth, the high porosity of IOS allows the infiltration of electrolyte which extracts holes rapidly so as to inhibit the photocorrosion of CCNCs.

Recently, several semiconductor materials, such as WO_3,[23,24] $BiVO_4$[24-26] and Fe_2O_3,[27] have been assembled into IOS and applied in water splitting system. However, as compared with thin film electrodes, the IOS based electrodes suffered from relatively low photocurrents.[23-27] The crux is distinguished as the poor charge transfer in IOS comprising fine nanocrystals, which dramatically compromises their advantageous light absorption and charge separation.

[a] *Key laboratory of advanced ceramics and machining technology of ministry of education, School of Materials Science and Engineering, Tianjin University, Tianjin 300072, People's Republic of China. E-mail: lingt04@tju.edu.cn, xwdu@tju.edu.cn.*

‡*These authors contributed equally.*

Electronic Supplementary Information (ESI) available: Schematic diagram of the assembly process of the IOS electrode, side-view SEM and TEM images of CdS IOS, SEM images and XRD pattern of CdS film, structural models for the FDTD simulation, SEM, XRD and U-V absorption characterizations of CdS/CdSe IOS. See DOI: 10.1039/x0xx00000x

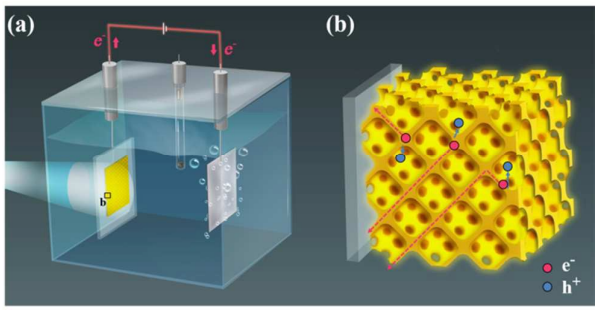

Scheme 1. (a) Experimental setup for PEC water splitting, (b) schematic structure of the IOS photoanode.

In the present work, we manage to prepare highly conductive IOS of CCNSs and demonstrate its superiority in water splitting. First, we develop a two-step process to fabricate well-designed IOS of CCNSs, where primary IOS is produced via co-deposition and calcination, then electrodeposition and annealing treatments are employed to improve the electrical conductivity. Next, we apply IOS to water splitting and realize efficient hydrogen production. Specifically, the photocurrent density of pure CdS IOS is 3.1 times that of the thin film electrode, the stability is even higher than CdS photoanodes with surface passivation and/or co-catalysts, and after being coated with a CdSe layer, the photocurrent density and hydrogen production rate reaches 10.5 mA cm^{-2} and 98.2 μmol h^{-1} cm^{-2}, respectively, which are the top values achieved by CCNCs. Finally, we quantitatively investigate the mechanism that IOS promotes PEC performance, and find that IOS can transmit electrons as quick as think film does, while its light absorption and charge separation are 1.2 and 2.4 times that of thin film, respectively, as a result, IOS achieves the unprecendent PEC performance.

Experimental

Synthesis of IOS.

PS spheres and water-stable CdS QDs were co-assembled on a fluorine-doped tin oxide (FTO) substrate following a procedure reported in our previous work.[28] Then the obtained film was calcined at 400 °C in air for 30 min to remove the PS spheres and produce the original CdS IOS. Afterwards, an extra CdS layer was grown on the IOS by electrodeposition (ED) to improve the electronic conductivity. The electrolyte for ED was prepared by dissolving 0.055 M $CdCl_2$ and 0.19 M sulphur powder in 50 ml dimethyl sulfoxide at 110 °C. The ED time and current density were set as 10 min, and 0.5 mA cm^{-2}, respectively. At last, annealing treatment was conducted at 500 °C for 30 min in nitrogen.

Synthesis of CdS film.

CdS film was synthesized as a reference through a physical vapor deposition (PVD) process. 0.1 g CdS powder was put into the middle of a tube furnace, heated to 710 °C, held at the temperature for 30 min, and a FTO substrate was placed downstream in the low temperature area. Nitrogen carrier gas was introduced into the furnace tube at a flow rate of 300 standard cubic centimeter per minute during the deposition, and the total pressure was adjusted to 8 torr.[29] Finally, a film with a thickness of ~2 μm could be obtained at the distance ~14 cm away from the CdS source.

PEC measurements for water splitting.

The PEC hydrogen evolution was tested in a standard three-electrode system under simulated AM 1.5 solar illumination (Scheme 1a). The IOS or thin film deposited on FTO substrate served as the work electrode, a Pt plate as the counter electrode, and Ag/AgCl as the reference electrode. An aqueous solution of 0.25 M Na_2S/0.35 M Na_2SO_3 was used as electrolyte and sacrificial reagent.[15,17,18]

Characterizations.

The morphologies of the IOS and thin film were observed by a Hitachi S-4800 scanning electron microscope (SEM) at an accelerating voltage 5 kV and a Technai G2 F20 transmission electron microscope (TEM) with a field emission gun operated at 200 kV. The composition was analyzed by an EDS module attached on SEM. XRD measurement was carried out using a Bruker D/max 2500 v/pc diffractometer. The diffuse reflectance spectra and transmittance spectra were examined by a Hitachi 3010 UV–vis absorption spectrometer with an integrating sphere. The linear sweep voltammogram measurements were examined by a Versastat 3 potentiostats electrochemistry workstation at a scan rate of 0.05 Vs^{-1}. A 300 W Xe lamp calibrated by a standard Si solar cell was used to simulate the 1 sun illumination (100 mW cm^{-2}). The incident light was irradiated from the FTO side. The incident photon to current conversion efficiency (IPCE) was measured with a tungsten quartz halogen light source, mono-chromator, filters, reflective optics to provide monochromatic light, mechanical chopper to modulate the light, and transition impedance amplifier to provide the test device signal to a digital source meter (Keithley 2611). Electrochemical impedance spectroscopy (EIS) measurements were performed on a Versastat 3 potentiostats electrochemistry workstation with a frequency range from 0.1 Hz to 100 kHz at 0 V vs Ag/AgCl. The actual H_2 production was detected every half an hour using a gas chromatograph (GC-2014C) possessing a thermal conductivity detector (TCD) and a molecular sieve 5 A column.

FDTD simulation.

Light absorption in CdS IOS and thin film was simulated using commercial software, Lumerical. The parameters of CdS material was adopted from the literature.[30] The absorption profiles were calculated based on the formula $P_{abs}=-0.5\omega|E|^2$ imag(ε), where P_{abs} is the power absorption per unit volume, ω the angular frequency, |E| the electric field intensity and imag(ε) the imaginary part of the permittivity. Then, the number of the absorbed photon can be calculated by $P_n=P_{abs}*\lambda/hc$, where P_n is the number of absorbed photon per unit volume, λ the wavelength, h the Planck constant, and c the speed of light.

Results and discussion

CdS IOS was prepared via co-deposition and then calcination (Figure S1).[28] Figure 1a presents a top-view scanning electron microscope (SEM) image of the original IOS with pore size of 250 nm and wall thickness about 15 nm. Electrodeposition and annealing treatments were further adopted to improve the light absorption (Figure S4) and electrical conductivity of the original IOS. As shown in Figure 1b, the wall thickness increased approximately to 60 nm via the post-treatments. Notably, this value is smaller than the hole diffusion length of CdS (100 nm).[31] The side-view SEM image (Figure S2) indicates that 2-μm-thick IOS contacts tightly with the conductive glass substrate, and provides a direct pathway for electron transport. Energy dispersive spectrometer (EDS) and x-ray diffraction (XRD) patterns illuminate that CdS IOS possesses stoichiometric composition and a hexagonal phase structure (Figure 1c), respectively, coinciding with the selected area electron diffraction (SAED) pattern (the inset of Figure S3a). The transmission electron microscope (TEM) and high resolution TEM images (Figure S3) show that the final IOS consists of highly crystalline nanocrystals with the grain size of 40-50 nm. This implies that the photo-generated holes can reach the electrolyte after the migration in just one nanocrystal, which is beneficial for hole extraction. Moreover, the increase in grain size and wall thickness after electrodeposition and annealing treatments directly result in the improved light absorption and high conductivity of the IOS, and finally lead to the improvement of the PEC performance and stability (Figure S5).

Mott-Schottky (M-S) analysis was conducted to identify the charge transfer capability of the original and final CdS IOSs. From the slope of M-S plots (Figure 1d), the donor concentrations (N_d) of the original and the treated IOSs were calculated as 6.8×10^{15} and 2.3×10^{16} cm^{-3}, respectively. Hence, the electrical conductivity of IOS is remarkably promoted after the electrodeposition and annealing treatments, and the carrier concentration of IOS attains the same order of magnitude as that of CdS film with columnar crystals (5×10^{16} cm^{-3}).[32]

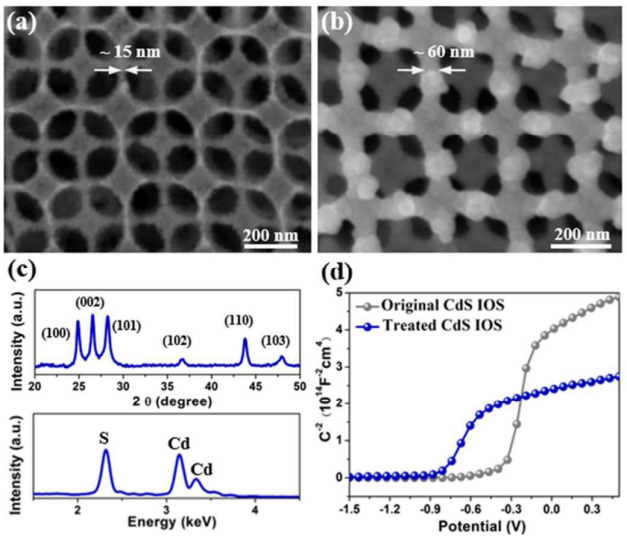

Fig. 1 Characterizations of IOS. (a) and (b) are top-view SEM images of the original CdS IOS (after co-deposition and calcination) and final IOS (after electrodeposition and annealing), respectively. (c) XRD (top) and EDS (bottom) patterns of the final IOS, respectively. (d) Mott-Schottky plot of the original and final IOS electrodes measured in a two-electrode system with a Pt film coated conductive glass substrate as the counter electrode.

The treated CdS IOS was employed as the photoanode for PEC hydrogen evolution and tested in a standard three-electrode system under AM 1.5 solar radiation (Scheme 1). We choose an optimized vacuum evaporation 2 μm-thick CdS film

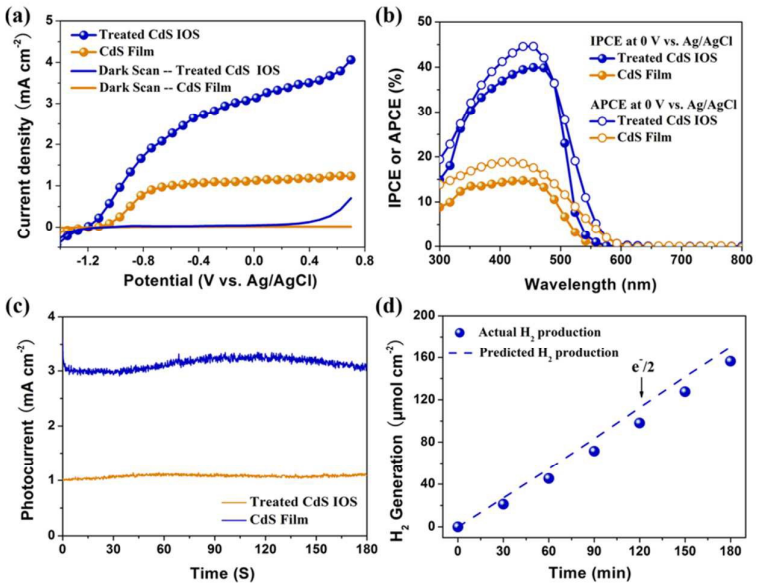

Fig. 2 PEC performances of the CdS IOS and film electrodes. (a) Linear sweep voltammograms measurements under 1 sun AM1.5G illumination and in the dark. (b) IPCE and APCE spectra under 1 sun AM1.5G illumination, at 0 V vs Ag/AgCl reference electrode. (c) and (d) are photocurrent stability and time evolution of the IOS photoanode at 0 V versus RHE under AM 1.5 illumination, respectively. The dashed line in (d) is the calculated hydrogen evolution assuming 100% faradaic efficiency.

Table 1. The H_2 generation stabilities of the reported cadmium chalcogenide based electrodes.

Electrode	During time and maintaining potential	J_0 (mA cm^{-2})	Stability (J/J_0)	Reference
CdS IOS	180 min, 0 V vs Ag/AgCl	3.1	~1	This work
Multi-segmented CdS-Au nanorods	35 min, 0 V vs Ag/AgCl	10.5	~0.963	15
TiO_2 nanowire/CdS/CdSe/ZnS	30 min, 0 V in a two-electrode cell	2	~0.9	18
TiO_2 nanoparticles/CdS/CdSe	30 min, 0 V in a two-electrode cell	1.4	~0.86	18
TiO_2 inverse opals/CdS	5 min, 0 V vs Ag/AgCl	4.8	~0.93	19
ZnO nanowire/CdS/CdSe	180 min, 0.6 V vs RHE	11.9	~0.68	17
ZnO nanowire/CdS/CdSe/IrO_x	180 min, 0.6 V vs RHE	13.9	~0.95	17

as the control sample (Figure S6-S8). Figure 2a displays the photocurrent density–potential (*J–V*) curves in the dark and under illumination, respectively. The IOS photoanode presents a higher photocurrent density than that of the CdS film. At 0 V versus Ag/AgCl, the IOS electrode achieves a photocurrent density of 3.1 mA cm^{-2} which is 3.1 times that of the film electrode (1 mA cm^{-2}). Moreover, the IOS electrode exhibits early potential onset comparable to the planar film, which reflects a high photovoltage and less carrier recombination in the IOS structure. However, the CdS film electrode with columnar crystals shows a plateau photocurrent, which arises from the relatively good electronic conductivity comparable to IOS electrode.

Incident photon to current conversion efficiency (IPCE) results are given in Figure 2b. The curves for both samples show an onset of photocurrent at 530 nm, corresponding to the band gap excitation of CdS. Obviously, the IOS electrode displays higher IPCE values in the overall spectrum region, with a maximum IPCE of ~39% at 400–500 nm, which is 3-fold as high as the film electrode (~13%). The absorbed photon to current conversion efficiency (APCE) value of the IOS electrode is much higher than that of the film in the whole tested wavelength. The IOS electrode achieves a maximum APCE of 45% at 480 nm, which is about 2.4 times that of the CdS film.

The stability of the IO and film electrodes were evaluated at 0 V vs Ag/AgCl under continuous illumination of AM 1.5 (Figure 2c). The photocurrent density-time (*J-t*) curve of IOS kept stable for 3 hours without obvious decay (J/J_0~1). XRD and SEM characterizations show that the crystal structure and morphology of the treated CdS IOS were well preserved after the stability test (Figure S9). In order to improve the photo-stability of CCNSs in PEC application, CCNSs were usually loaded onto the surface of TiO_2 or ZnO to enhance charge separation.[17-19] Moreover, the surface coating of CCNSs with ZnS was proved to be an extremely effective route to passivate the surface defect states of CCNSs.[18] Recently, the oxygen evolution cocatalyst IrO_x was added to enhance the hole transfer and reduce the charge recombination.[17] Comparison with these successfully designed CCNCs-based electrodes,[17,18] the IOs electrode exhibits even better stability, as summarize in Table 1. Notably, the stability of the treated IOS is even comparable to the planar film with much less surface area and high conductivity, indicating a superior charge separation ability of the IOS.

Moreover, the theoretical hydrogen production versus time can be estimated according to the *J-t* curve by assuming faradaic efficiency as 100%, while the actual H_2 production rate can be directly measured and determined as 45 μmol h^{-1} cm^{-2} by gas chromatography. As shown in Figure 2d, the theoretical prediction matches the experimental measurements very well, indicating that almost all of photoelectrons contribute to the reduction of hydrogen.

To understand the origin of the excellent PEC performance, we detected the light absorption and charge separation of IOS with a thin film as reference. The diffuse reflection spectra presented in Figure 3a illustrate that the surface reflectance of IOS (~ 15%) is much lower than that of thin film (~25%) in the wavelength range between 350 and 500 nm (beyond the intrinsic absorption of CdS), revealing that the ordered void arrays can suppress surface reflection drastically. Moreover, IOS exhibits negligible light transmittance (Figure 3b). Resultantly, IOS achieves much higher light absorption than its film counterpart in the whole wavelength range (Figure 3c and Figure S10).

Finite-difference-time-domain (FDTD) simulations were performed to understand the experimental results. Figures 3d and 3e show the simulated distribution of absorbed photons in CdS film and IOS, respectively, under 500 nm transverse electric (TE)-polarized illumination from the FTO side (see simulation models in Figure S11). The numbers of absorbed photons decreases linearly with increasing penetrating depth in both samples, however, the decay rate of the two samples are different. As shown in the enlarge images in Figures 3f and 3g, the number of the absorbed photons in IOS is at least 2 orders of magnitude as large as that in thin film at the same penetrating depth. Further simulation on electromagnetic field distribution reveals that the enhancement of light absorption in IOS mainly arises from the multi-scattering effect (Figure S12).

Next, charge separation dynamics in the photoanodes was characterized by the electrochemical impedance spectroscopy (EIS). Figure 4a shows the Nyquist plots (circle symbols) tested at 0 V vs Ag/AgCl under AM 1.5 illumination. The corresponding equivalent circuit model is shown in the inset of Figure 4a, where R_s represents the resistance of the electrolyte, CPE the capacitance phase element and R_{ct} the charge transfer resistance between the photoanode and the

electrolyte. By fitting the Nyquist plots with the given model (Figure 4a, line),

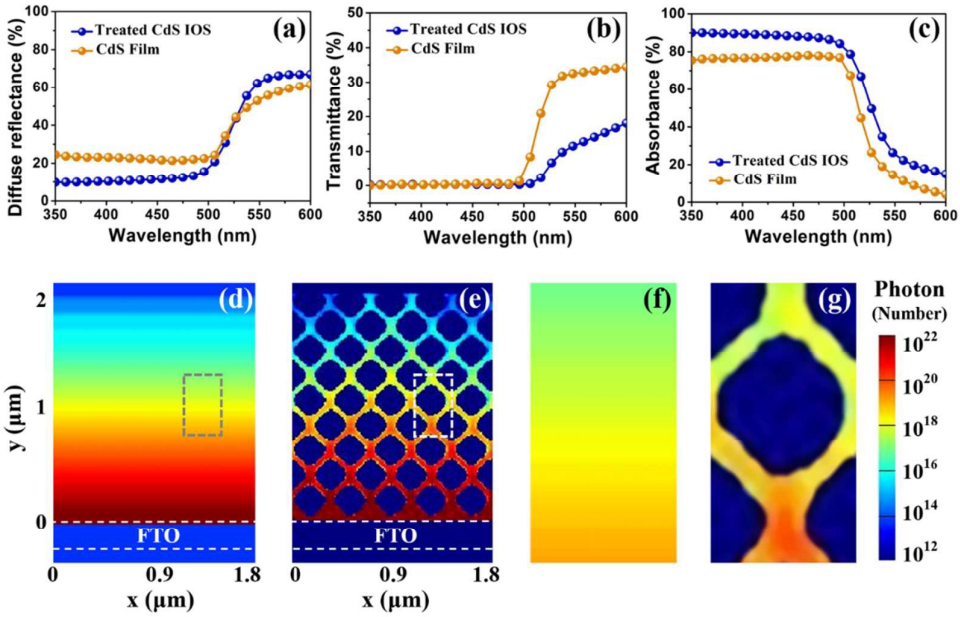

Fig. 3 Optical performance of IOS and film. (a)-(c) are diffuse reflectance spectra, transmittance spectra, and absorbance spectra of IOS and film, respectively. (d) and (e) are simulated photon number distributions of film and IOS, respectively, under TE-polarized illumination at 500 nm. (f) and (g) are enlarged images of the regions labeled in (d) and (e), respectively.

the values of R_{ct} in the IOS and film electrodes can be determined as 760 and 1835 Ω, respectively, indicating that the hole transfer through the solid/liquid interface is more favorable in the IOS electrode. Moreover, the electron lifetime As shown in Figure 4b, the f_{max} for IOS is 20 Hz, much smaller than that for thin film (610 Hz). The calculated electron lifetimes of IOS and film are 7.9 and 0.26 ms, respectively. A nearly 30-fold enhancement of the electron life time for the IOS sample suggests much slower electron-hole recombination occurring in the IOS electrode, indicating a rather advantageous charge separation process arising from the fast hole transfer.

According to the above experimental results, we can distinguish the role of IOS in each step of PEC process (light absorption, charge separation, charge transfer and so on), and understand its effect on the final performance. The IPCE value of photoelectrode can be expressed as,[33, 34]

$$\mathrm{IPCE} = \eta_{abs} \times \mathrm{APCE} = \eta_{abs} \times \eta_{sep} \times \eta_{trans} \quad (2)$$

where η_{abs}, η_{sep} and η_{trans} are the light absorption, charge separation and transfer efficiencies, respectively. Owing to the anti-reflection and multi-scattering effects of the ordered porous structure, IOS achieves an average light absorption of 1.2 times as high as that of the thin film (between 400-500 nm wavelength). On the other hand, the large surface area and thin wall thickness (less than the hole diffusion length) of IOS leads to fast hole transfer and then a charge separation efficiency of ~2.4 times as large as that of the film counterpart. The two factors jointly elevate IPCE of the IOS electrode to a value ~2.9 times (1.2×2.4) that of CdS film, which is almost consistent with the experimental value (~3). Therefore, the third term, charge transfer efficiency of IOS, should be same with that of thin film. This conclusion is supported by the similar carrier concentrations in IOS (2.3×10^{16} cm^{-3}) and thin film (5×10^{16} cm^{-3}). The high carrier concentrations affirm fast (τ_n) of the photoanodes can be calculated from the Bode phase plots (Figure 3b), using the equation,[19,35,36]

$$\tau_n = 1/(2\pi f_{max}) \quad (1)$$

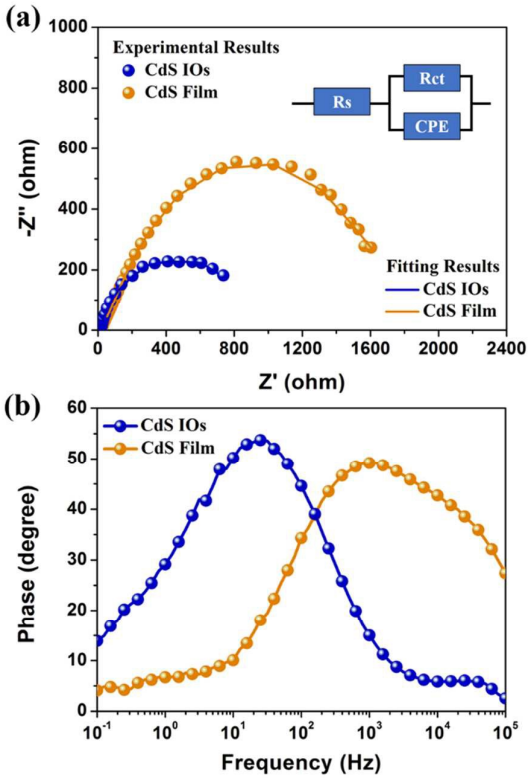

Fig. 4 Charge separation dynamics in the IOS and film photocathodes. (a) is Nyquist plots of the EIS spectra measured at 0 V vs Ag/AgCl, and the inset is the equivalent circuit. (b) is Bode phase plots.

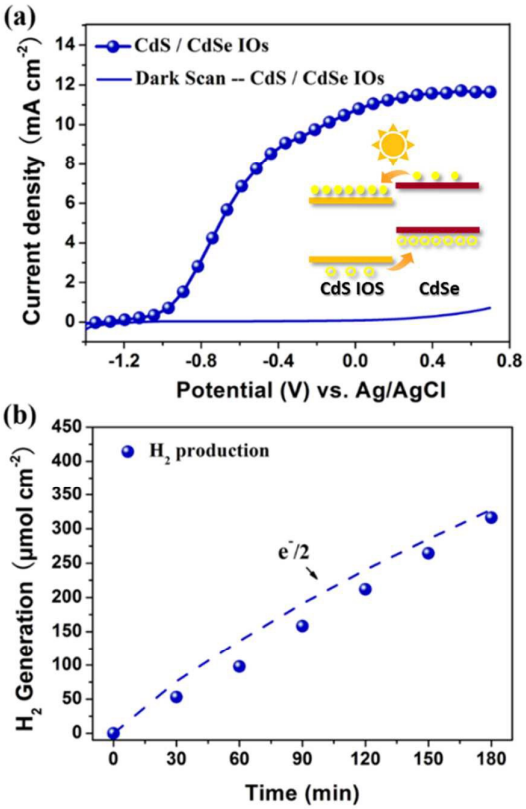

Fig. 5 PEC properties of CdS/CdSe IOS. (a) Linear sweep voltammograms measurements under 1 sun AM1.5G illumination (symbols and solid line) and in the dark (solid line). (b) Time evolution of hydrogen generation under 1 sun AM 1.5G illumination at 0 V vs. Ag/AgCl (symbols), where the dashed line represents the expected hydrogen production.

electron transfer, leading to a charge transfer efficiency of approximately 100% in both electrodes.

In order to extend the absorption range of the IOS electrode, a CdSe layer with the thickness of about 20 nm was electrodeposited onto CdS IOS (Figure S13). The CdS/CdSe IOS shows enhanced light absorption with an absorption edge at 700 nm (Figure S14). Moreover, the stepwise band structure of CdS/CdSe is advantageous for both light generated electron and hole. As a result, the CdS/CdSe IOS electrode exhibits a high PEC performance with a photocurrent density of 10.5 mA cm^{-2} and an actual H_2 generation rate of 98.2 μmol h^{-1} cm^{-2} at 0 V vs Ag/AgCl under 1 sun illumination (Figure 5), these values are among the highest performance achieved by pure cadmium chalcogenide materials in literature.[37-43] However, the PEC stability of this heterogeneous IOS (Figure S15) should be further improved.

Conclusions

We demonstrates that IOS can overcome the intrinsically slow hole transfer kinetics of CdS photoanode without compromising the light absorption. As a result, the IOS photoanode achieves water splitting efficiency 3.1 times that of the CdS film. Moreover, owing to fast hole transfer, the IOS photoanode exhibits a high stability, the photocurrent density keeps constant during 3 h continuously illumination. After being coated with a CdSe layer the Cd/CdSe IOS electrode brings about a photocurrent density as high as 10.5 mA cm^{-2} at 0 V vs the Ag/AgCl electrode under 1 sun illumination. Quantitative investigation illuminates that IOS achieves charge separation efficiency 2.4 times that of thin film, light absorption capacity 1.2 times that of thin film, and charge transfer efficiency same with thin film. These exciting results suggest that IOS of CCNCs is promising for efficient and stable visible light water splitting.

Acknowledgements

This work was supported by The National Basic Research Program of China (2014CB931703), the Natural Science Foundation of China (Nos. 51402084 and 21103224), and the Natural Science Foundation of Tianjin city (15JCYBJC18200).

Notes and references

1 M.Gratzel, *Nature,* **2001**, 414, 338-344.
2 N. S. Lewis and D. G. Nocera, *Proc. Natl. Acad. Sci. U.S.A.,* **2006**, 103, 15729-15735.
3 C. G. Morales-Guio, S. D. Tilley, H. Vrubel, M. Graetzel and X. Hu, *Nat. Commun.,* **2014**, 5, 0359.
4 A. Paracchino, V. Laporte, K. Sivula, M. Graetzel and E. Thimsen, *Nat. Mater.,* **2011**, 10, 456-461.
5 Z. Li, W. Luo, M. Zhang, J. Feng and Z. Zou, *Energy Environ. Sci.,* **2013**, 6, 347-370.
6 A. F. K. Honda, *Nature,* **1972**, 238, 37-38.
7 C. X. Kronawitter, L. Vayssieres, S. Shen, L. Guo, D. A. Wheeler, J. Z. Zhang, B. R. Antoun and S. S. Mao, *Energy Environ. Sci.,* **2011**, 4, 3889-3899.
8 L. Liu, S. K. Karuturi, L. T. Su and A. I. Y. Tok, *Energy Environ. Sci.,* **2011**, 4, 209-215.
9 Z. Zhang, R. Dua, L. Zhang, H. Zhu, H. Zhang and P. Wang, *ACS Nano,* **2013**, 7, 1709-1717.
10 A. Kargar, Y. Jing, S. J. Kim, C. T. Riley, X. Pan and D. Wang, *ACS Nano,* **2013**, 7, 11112-11120.
11 P. V. Kamat, J. Phys. *Chem. C.,* **2008**, 112, 18737-18753.
12 G. Hodes, *J. Phys. Chem. C.,* **2008**, 112, 17778-17787.
13 W. W. Yu, L. H. Qu, W. Z. Guo and X. G. Peng, *Chem. Mater.,* **2003**, 15, 2854-2860.
14 A. J. Nozik, *Physica E.,* **2002**, 14, 115-120.
15 X. Wang, C. Liow, D. Qi, B. Zhu, W.R. Leow, H. Wang, C. Xue, X. Chen and S. Li, *Adv. Mater.,* **2014**, 26, 3506-3512.
16 H. B. Yang, J. Miao, S.-F. Hung, F. Huo, H. M. Chen and B. Liu, *ACS Nano,* **2014**, 8, 10403-13.
17 M. Seol, J. W. Jang, S. Cho, J. S. Lee and K. Yong, *Chem. Mater.,* **2013**, 25, 184-189.
18 P. Rodenas, T. Song, P. Sudhagar, G. Marzari, H. Han, L. Badia-Bou, S. Gimenez, F. Fabregat-Santiago, I. Mora-Sero, J. Bisquert, U. Paik and Y. S. Kang, *Adv. Energy Mater.,* **2013**, 3, 176-182.
19 C. W. Cheng, S. K. Karuturi, L. J. Liu, J. P. Liu, H. X. Li, L. T. Su, A. I. Y. Tok and H. J. Fan, *Small,* **2012**, 8, 37-42.
20 R. Rengarajan, D. Mittleman, C. Rich and V. Colvin, *Phys. Rev. E.,* **2005**, 71, 016615.

21 S. Guldin, S. Huttner, M. Kolle, M. E. Welland, P. Mueller-Buschbaum, R. H. Friend, U. Steiner and N. Tetreault, *Nano Lett.,* **2010**, 10, 2303-2309.
22 O. Toader and S. John, *Phys. Rev. E.,* **2004**, 70, 046605.
23 M. Ma, J. K. Kim, K. Zhang, X. Shi, S. J. Kim, J. H. Moon and J. H. Park, *Chem. Mater.,* **2014**, 26, 5592-5597.
24 X. Chen, J. Ye, S. Ouyang, T. Kako, Z. Li and Z. Zou, *ACS Nano,* **2011**, 5, 4310-4318.
25 M. Zhou, J. Bao, Y. Xu, J. J. Zhang, J. F. Xie, M. L. Guan, C. L. Wang, L. Y. Wen, Y. Lei and Y. Xie, *ACS Nano,* **2014**, 8, 7088-7098.
26 L. Zhang, E. Reisner and J. J. Baumberg, *Energy Environ. Sci.,* **2014**, 7, 1402-1408.
27 Y. Qiu, S.-F. Leung, Q. Zhang, B. Hua, Q. Lin, Z. Wei, K.-H. Tsui, Y. Zhang, S. Yang and Z. Fan, *Nano lett.,* **2014**, 14, 2123-9.
28 T. Ling, S. A. Kulinich, Z.-L. Zhu, S.-Z. Qiao and X.-W. Du, *Adv. Funct. Mater.,* **2014**, 24, 707-715.
29 P.-F. Yin, T. Ling, Y.-R. Lu, Z.-W. Xu, S.-Z. Qiao and X.-W. Du, *Adv. Mater.,* **2015**, 27, 740-745.
30 P. P. Sahay, R. K. Nath and S. Tewari, *Cryst. Res. Technol.,* **2007**, 42, 275-280.
31 J. E. Allen, G. Yi, J. P. Romankiewicz, J. L. Lensch, S. J. May, T. W. Odom, B. W. Wessels and L. J. Lauhon, *IEEE Device Research Conference*, University Park PA; IEEE: Piscataway, NJ, **2006**; pp 289-290.
32 I. L. Eisgruber, J. E. Granata, J. R. Sites, J. Hou and J. Kessler, *Sol. Energ. Mat. Sol. C.,* **1998**, 53, 367-377.
33 T. W. Kim and K.-S. Choi, *Science,* **2014**, 343, 990-994.
34 P. M. Rao, L. Cai, C. Liu, I. S. Cho, C. H. Lee, J. M. Weisse, P. Yang and X. Zheng, *Nano Lett.* **2014**, 14, 1099-1105.
35 R. Kern, R. Sastrawan, J. Ferber, R. Stangl and J. Luther, *Electrochim. Acta,* **2002**, 47, 4213-4225.
36 Y. H. Jang, X. Xin, M. Byun, Y. J. Jang, Z. Lin and D. H. Kim, *Nano Lett.,* **2012**, 12, 479-485.
37 S. Choudhary, S. Upadhyay, P. Kumar, N. Singh, V. R. Satsangi, R. Shrivastav and S. Dass, *Int. J. Hydrogen Energ.,* **2012**, 37, 18713-18730.
38 Y. Du, B. Chen, Z. Yin, Z. Liu and H. Zhang, *Small,* **2014**, 10, 4727-4734.
39 X. Guo, J. Zhu, H. Wei, S.-T. Lee, Y. Li and J. Tang, *Nanotechnology,* **2015**, 26, 015203.
40 Y. K. Kim, M. Kim, S.-H. Hwang, S. K. Lim, H. Park and S. Kim, *Int. J. Hydrogen Energ.,* **2015**, 40, 136-145.
41 P. K. Mahapatra and B. B. Panda, *Chalcogenide Lett.,* **2010**, 7, 477-483.
42 M. Wang, J. Jiang, J. Shi and L. Guo, *Appl. Mater. Inter.,* **2013**, 5, 4021-4025.
43 C. Bao, G. Zhu, J. Yang, M. Liu, R. Zhang and X. Shen, *Dalton T.,* **2015**, 44, 1465-1472.